

COMPUTATIONAL AND EXPERIMENTAL ANALYSIS OF THE ACTIVE MORPHING WING CONCEPT

D.D. Smith*, M.H. Lowenberg*, D.P. Jones*, M.I. Friswell**

***University of Bristol, Bristol, BS8 1TR, UK**

****Swansea University, Singleton Park, Swansea, SA2 8PP, UK**

Keywords: *Morphing, Winglet, Euler, CFD, Experimental aerodynamics*

Abstract

High fidelity computational and experimental analysis has been performed upon a conventional aircraft wing with variable outer twist and dihedral angle. Results are aimed to confirm initial trends in aerodynamic and structural efficiency observed through previous optimisation studies. Computational results are obtained with the DLR Tau computational fluid dynamics code and experimental testing has been performed in the University of Bristol low speed wind tunnel. Outer twist variation of $\pm 3^\circ$ and dihedral angles from planar up to 90° C-wing geometries are tested for a range of incidence angles. Results demonstrate the potential effectiveness of a number of differing configurations and emphasise the sensitivity of the outcome to the analysis method.

1 Introduction

A variety of wing tip designs have been proposed as a means for reducing the vortex-induced drag of aircraft wings. Minimising the induced drag is an area of intense research as the industry strives to reduce fuel consumption and provide more economic and environmentally friendly aircraft. In climb conditions with high lift coefficients, induced drag can account for up to 90% of the total aircraft drag, and typically 30-40% in cruise. Since Richard Whitcomb proposed the complex Whitcomb winglet in 1976 [1], achieving induced drag reductions of up to 20%, more novel solutions such as multi-winglets [2], wing

grids [3] and C-wings [4] have been investigated. In 2005 the Morphing Wings research group at the University of Bristol proposed a morphing winglet, or Morphlet, consisting of two outboard partitions that could be reconfigured in twist and cant angle during flight. The Morphlet system could be retrofitted to an existing commercial narrowbody aircraft with fixed sweep and camber in order to improve fuel efficiency through drag reduction. Optimisation studies were performed [5][6] using low fidelity methods to ascertain the benefits in drag reduction through re-optimising the aircraft wing span loading. Initial results revealed that through morphing the wing tips for each unique flight phase, a consistent 6% specific air range (SAR) improvement was achieved, by virtue not only of reducing the induced drag via wake manipulation, but also by reconfiguring the span loading for each phase so as to minimise the wing structural weight and thus the aircraft maximum take off weight (MTOW).

A number of wing tip designs have been analysed using the Lanchester-Prandtl Lifting Line theory [7] and potential methods, a popular choice given their relatively low computational cost. These methods can be successfully applied to induced drag analysis as the aircraft vortex sheet structure that leaves the trailing edge is independent of viscosity provided there is no separation [8]. Therefore these lower fidelity methods provide fast and accurate solutions. Such methods are also particularly useful for optimisation studies in the conceptual design phase where large numbers of geometric combinations are to

be investigated. With regard to drag analysis, the main weakness with these low fidelity methods, however, is that they model the wake based upon the geometry and do so prior to solving. In order to replicate a more accurate freely deforming wake an advanced solution method is required. In addition to this, experimental testing is required to validate all computational results. Therefore in order to analyse the trends that have been observed, further results are derived from two methods - high level computational fluid dynamics (CFD) and experimental low speed wind tunnel testing. This paper presents initial results from these ongoing activities.

2 Computational Analysis

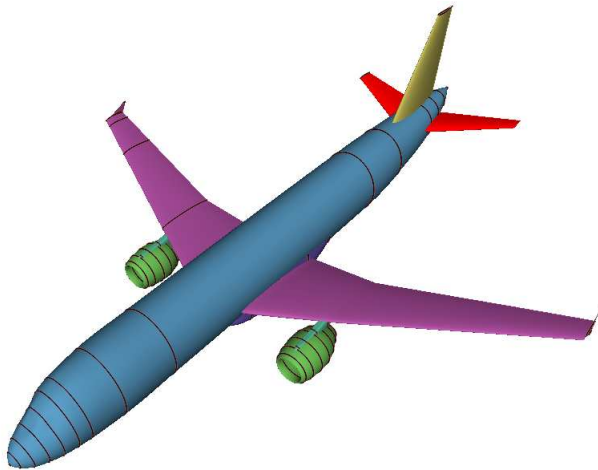


Fig. 1 Initial Sumo aircraft model.

High fidelity CFD results are obtained using the Tau CFD code [9]. An Euler solver is used for aerodynamic computation. Euler solvers are less computationally expensive in comparison to full Navier-Stokes as they neglect viscosity from the analysis, but consequently do not capture boundary layer growth or predict stall. However as the main parameters of interest, namely the induced drag and spanwise lift, are fundamentally inviscid, these are able to be computed. The aircraft model investigated replicates a conventional commercial passenger jet along with the Morphlet system of the previous work, consisting of two outboard panels, one replacing the aileron

partition and a further partition outboard. These partitions vary in dihedral angle from planar up to 90° and in twist by $\pm 3^\circ$. However the spans of the two morphing outboard partitions are equal and fixed for this analysis and represent the final third of the wing span in length. For both methods of testing, the two morphing partitions are modelled in sequence, such that the twist and dihedral angles accumulate for the outer of the two partitions. For the cases with $+3^\circ$ twist or 90° dihedral, the outer partition will have an absolute twist of 6° or 180° dihedral respectively.

The meshes generated for Tau are converted from Sumo meshes [10]. An initial Sumo mesh for a conventional commercial passenger jet, as shown in Figure 1, is taken as the baseline aircraft to be analysed. For the Tau mesh, the fuselage, nacelles, empennage and wing fences were removed and two morphing outer partitions were shaped onto the wing tip. The Tau mesh generated for the planar wing case is given in Figure 2.

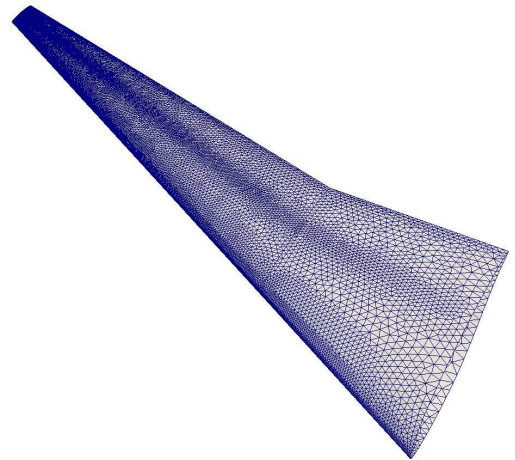


Fig. 2 Planar wing mesh generated for Tau.

The computational results are generated to replicate flight conditions typical of initial cruise. The Mach number for analysis has been set to 0.78 and atmospheric conditions are input for a flight altitude of 35,000ft. A range of incidence angles are investigated to create result polars, namely $-5, 0, 2, 5, 10$ and 15° . Meshes are generated for the planar wing with the outer twist angles of both morphing partitions simultaneously varying through angles of $-3, -1.5, 0, 1.5$ and 3° .

In addition, meshes are generated with the two morphing partitions deflecting with dihedral angles of 0, 30, 45, 60 and 90° from the planar configuration with zero outboard twist. The wing mesh with 45° outer partition dihedral angle is given in Figure 3.

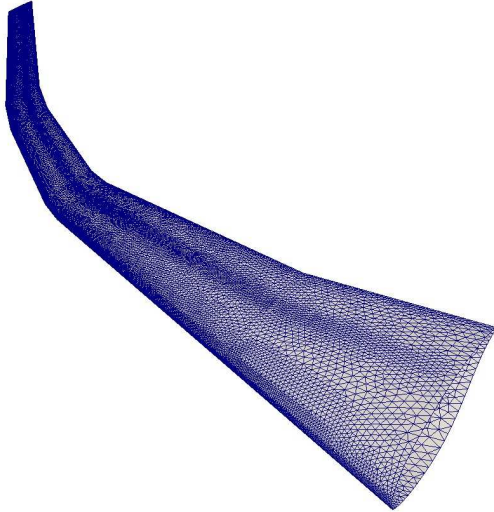


Fig. 3 Tau mesh with 45° dihedral on both outer morphing partitions.

3 Experimental Testing

Experimental testing is an important tool required to validate all computational results. With current technology, vortex lattice methods and computational fluid dynamics remain attractive and relatively inexpensive tools to use for analysis of aircraft wings. However they still retain weakness with regard to the simulation of real life flow conditions, such as separation, turbulence and boundary layer growth. Experimental testing therefore remains a primary analysis tool for capturing such effects and along with flight testing and computational results is a fundamental tool in aircraft design. In itself, experimental wind tunnel testing also contains sources of error, with regard to the effects of the tunnel and model support on the model and airflow as well as potential calibration and Reynolds Number discrepancies. Therefore the intention is for each of the multi-disciplinary optimisation, computational analysis

and experimental testing results to come together and each offer conclusions about the validity of the morphing wing concept.

3.1 Wind Tunnel Model

A wind tunnel model has been designed and constructed for testing in the University of Bristol 7 × 5ft Low Speed Wind Tunnel facility, a closed circuit, closed section wind tunnel. It was decided that the optimal construction for the model would be a half-wing model with fixed baseline inboard sections, complete with a number of detachable outboard partitions that vary, each with its specific twist and cant angle. The wing has been sized to span 65% of the wind tunnel cross-sectional width when fully planar, in accordance with standard wind tunnel testing recommendations from Barlow et al. [11]. This results in a wing of 8% scale relative to the datum aircraft from optimisation studies. The wing geometry assumes the same chordwise aerofoil sections as the vortex lattice and computational models. The model features two replaceable outboard partitions of equal span and scaled to replicate the span of the aileron partition for the true size aircraft.



Fig. 4 Planar wing CAD wind tunnel model design.

The model was designed using the Autodesk Inventor CAD software, as pictured in Figure 4. Three inboard sections, one modelling the fuselage-to-kink and two kink-to-aileron sections, were designed and constructed using Pro-lab WB-1222 [12] and strengthened using silver steel rods along the quarter and half chord

lines. The outboard sections were constructed via rapid-prototyping using ABS-M30 [13] and 2-Butanone was applied to the upper and lower surfaces to aerodynamically improve the smoothness of the model.

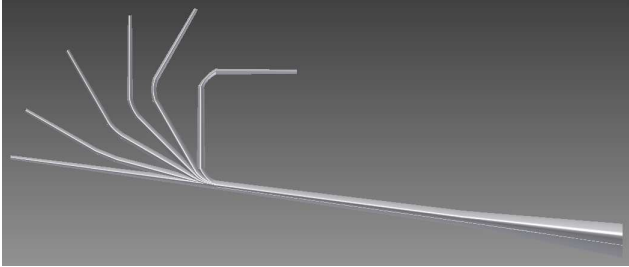


Fig. 5 Demonstration of the ranges of dihedral variation for the wind tunnel model.

The outboard partitions of the wing that reflect the morphing capability have been divided into four sections. These consist of two sections that are planar in geometry and may vary in twist angle from inboard to outboard and represent the aileron and outboard partitions. Two further sections are used, one inboard of each of these two partitions. These are 'fillet' sections that provide the variation in dihedral angle to the two outboard partitions. Five aileron and five outboard partitions have been manufactured, varying from -3° to $+3^\circ$ twist angle variation from root to tip. Additionally, six of each of the two fillet partitions have been produced, giving dihedral angle variation from fully planar up to 90° . This variation is displayed in Figure 5. This gives a total of 22 outboard parts made for the test, with the capability of assembling over 900 different schedule configurations. The wind tunnel model is displayed in Figure 6.

3.2 Test Conditions

The wind tunnel tests are conducted at 20m/s, giving a Reynolds number of 3.46×10^5 . Ideally the Reynolds number would be above 5×10^5 to ensure fully turbulent flow over the wing as per the real life aircraft, but due to restrictions on the wind tunnel model support, load cell and due to model flutter the wind speed could not be increased for this purpose. Incidence polars are



Fig. 6 Planar wing model configuration in the wind tunnel.

computed for each configuration, using a stepper motor to increase the incidence in 1° increments from -5 to 15° . Standard correction factors are applied relating to horizontal buoyancy, solid blockage, wake blockage and streamline curvature.

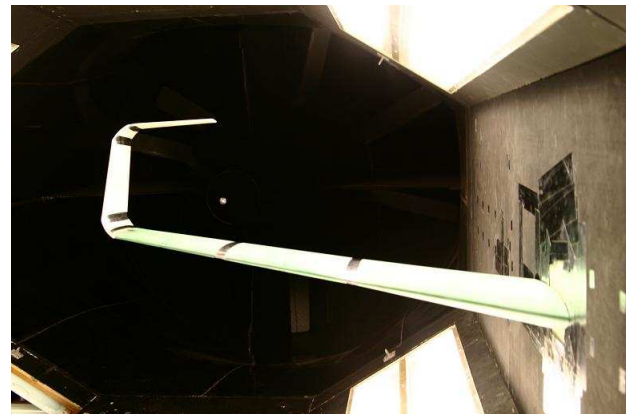


Fig. 7 C-wing configuration in the wind tunnel.

As with the computational analysis, parts with twist angles of -3 , -1.5 , 0 , 1.5 and 3° are fitted for both outboard partitions for the planar wing model. Then further runs are undertaken for partitions of 15 , 30 , 45 , 60 and 90° dihedral angle, as shown in the example in Figure 7, upon the outer partitions for the neutral twist planform.

4 Results

Results are presented for key parameter variations in incidence angle as the model was mor-

phed. These results aim to focus on particular trends observed in previous work that are hoped to be repeated with high fidelity analysis. The effect of morphing on the lift and drag coefficients is of particular interest, naturally. In addition the effect of twist and dihedral on the outer wing loading, and hence on the bending moments generated, is important as this bears significant impact upon the weight of the wing and hence, in tandem with the lift to drag ratio, the range. For this reason a specific air range (SAR) approximation has been made, which acts as a representation of the ratio between lift to drag improvement and wing weight increase. For each twist or dihedral angle quoted in figures, this represents the local variation from root to tip of both morphing partitions. The outermost partition thus has an absolute morphing angle double that of the quoted number.

Figure 8 gives the lift curve slopes observed for each of the analysed outer dihedral configurations. It displays both computational and wind tunnel results and thus acts as a comparison between the two methods. It can be seen that as expected the lower dihedral angled configurations produce more lift, by virtue of having a greater lift generating surface area. For the computational results, the 60° dihedral case is still able to generate lift comparable to that of the planar wing, however, and it is only at the maximum dihedral angle of 90° that lift is noticeably diminished. Additionally, the computational results exhibit a stronger lift curve slope gradient. This is due to the larger Reynolds and Mach number for the computational results, in addition to the lack of boundary layer separation in the inviscid solution for higher angles, and thus an increase in $C_{L\alpha}$ is to be expected. The graph also indicates that the stall behaviour is largely consistent across each dihedral angle variant.

The drag polar for varying outboard twist angles is given in Figure 9. These results obtained through wind tunnel testing show a trend for drag reduction as the wing twist increases outboard, suggesting that this gives a more optimal load distribution over the wing to minimise induced drag. However it can be seen that at higher angles

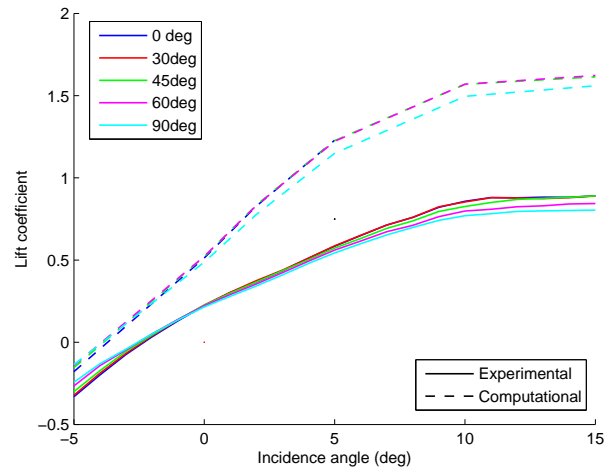


Fig. 8 Lift curve slope experimental and computational results for varying dihedral angles.

of incidence the flow separates earlier at the tips and the drag increases beyond that of more planar configurations. This occurs at an incidence angle of around 6°. As the twist angle increases, the angle of minimum drag can also be seen to slightly increase by 1°.

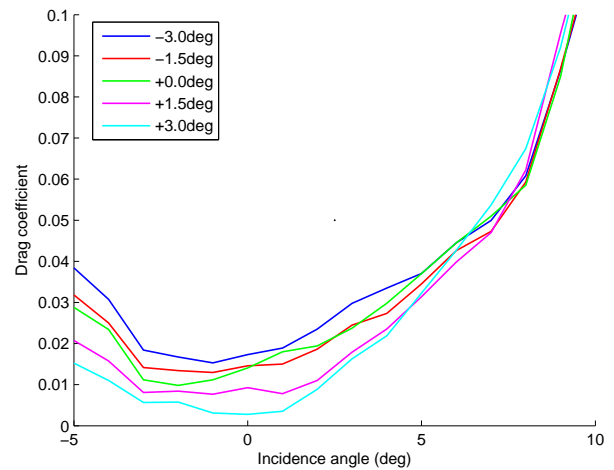


Fig. 9 Drag wind tunnel test results for varying twist angles.

Figure 10 offers another comparison between computational and experimental results, for the drag polar for differing dihedrals. Both sets of results demonstrate a trend for the drag to increase with dihedral angle, although the experimental results for the 45° and 60° dihedral angle mini-

imum drag values compare very favourably with a planar wing. However the 90° wing, despite having been seen to produce less lift, can also be observed to produce the highest drag values in general. This may be explained by the increase in pressure and interference drag caused by the increased deflection angle.

Despite not modelling the viscous drag components, the drag coefficient values are in general greater for the computational studies, possibly due to the greater lift coefficients observed in Figure 8. Indeed the computational results suggest that the minimum drag decreases with incidence angle. The wind tunnel results show a similar trend but for a clearly defined minimum drag angle of around -2 to -3°.

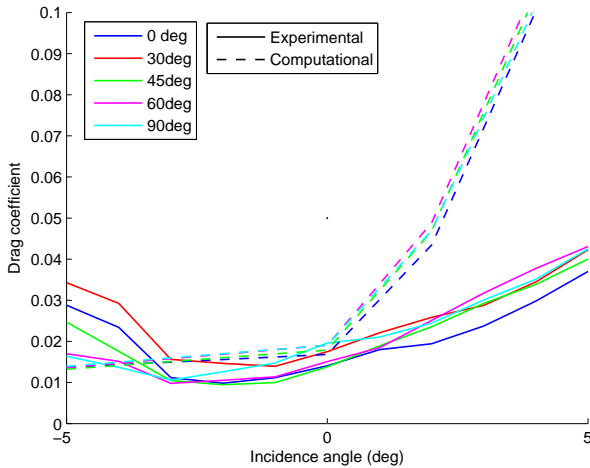


Fig. 10 Drag results comparison for varying dihedral.

The bending moment coefficients for each twist configuration are given in the graph in Figure 11. As expected the increased loading toward the outboard wing sections due to the increased twist drives up the bending moment coefficient. This will impact on the wing weight.

Figure 12 additionally gives the bending moment coefficient variation for the dihedral changes. There is a consistent trend for the bending moment to decrease as the dihedral angle is increased. As is the case with decreasing the outer wing twist, the inward shift of spanwise loading through increasing outer partition di-

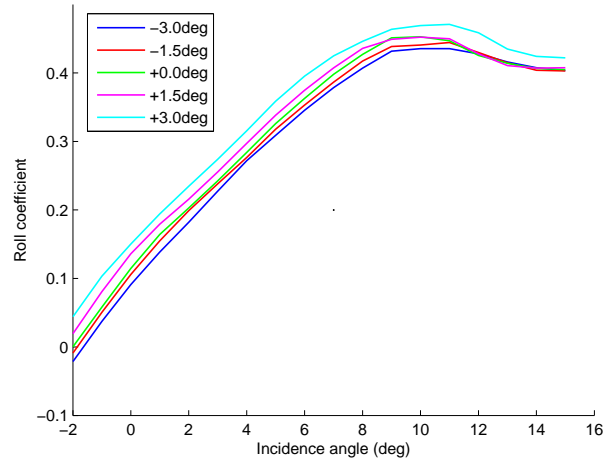


Fig. 11 Experimental results for bending moment coefficient variation with incidence for varying twist.

edral helps to reduce the bending moment at the wing root. These differences increase in magnitude as the angle of attack is increased, which is notable as these are the critical loads for which the wing is sized.

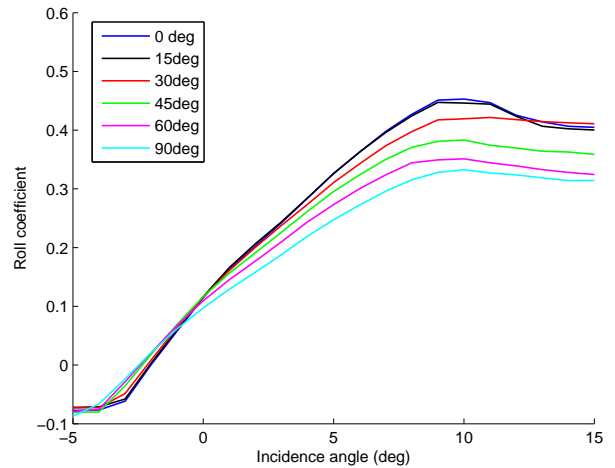


Fig. 12 Experimental results for bending moment coefficient variation with incidence for varying dihedral.

The lift curve slope and drag polars are combined to give the lift to drag variations in Figure 13. As expected from the previous results the 90° dihedral wing suffers the lowest lift to drag ratio. The optimal angle of attack appears to be

at around $0-2^\circ$ for each configuration.

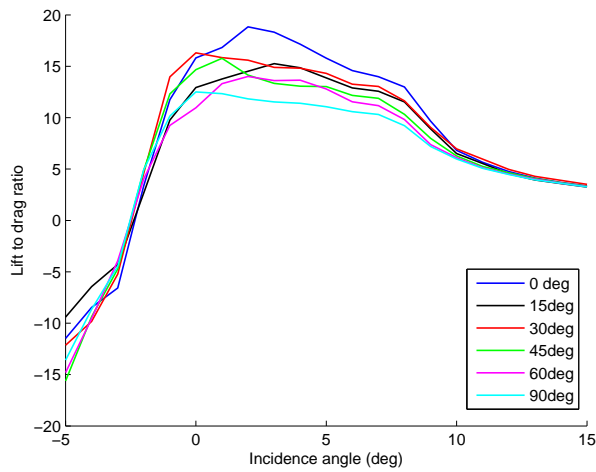


Fig. 13 Lift to drag ratio for various dihedral angles, experimental results.

The computational results largely back up the trends from wind tunnel tests. The Tau results given in Figure 14 predict a decrease in lift to drag with increasing outer dihedral. However Tau results show that the optimal lift to drag occurs at 0° with a sharp decrease beyond this incidence. There is also a convergence of lift to drag values as the incidence angle increases beyond 5° .

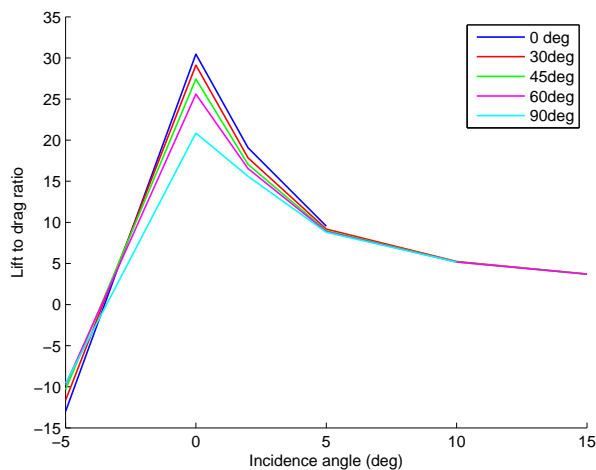


Fig. 14 Lift to drag ratio for various dihedral angles, computational results.

The preceding results all show conflicting trends, as was observed in previous work [6]. In-

creasing dihedral angle decreases the lift and increases the drag of the wing but reduces wing root bending moment. Similarly, increasing wing outer twist reduces the drag coefficient significantly but also suffers the penalty of bending moment increase. An attempt has been made to amalgamate the contrasting objectives by calculating a specific air range value that is a simple ratio of the lift to drag ratio and the bending moment coefficient observed at a nominal incidence angle. These results are presented in Figure 15 for experimental and Figure 16 for computational analysis.

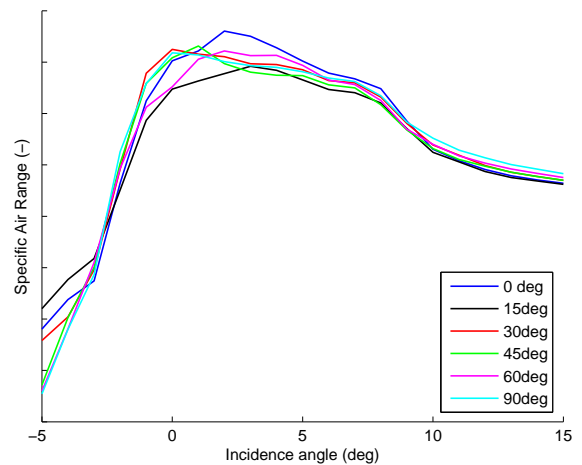


Fig. 15 Specific range for various dihedral angles, wind tunnel results.

Considering the experimental results, each configuration aside from the 15° deflection case achieves a similarly high specific air range peak in comparison with others, with the exception of the planar wing, which has a further peak at 2° as was seen with the lift to drag ratio. However looking at the computational results, there is a clear dominance for the high dihedral configurations throughout the alpha polar, and in fact furthermore the specific air range incremental improvements are also greater with increased dihedral angle.

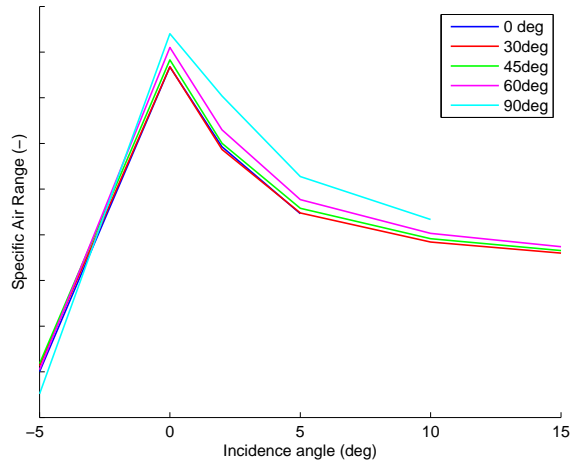


Fig. 16 Specific range for various dihedral angles, Tau results.

5 Conclusions and Future Work

Both computational and experimental results confirm the patterns observed in previous studies. As the wing configuration morphs, increased dihedral angles shift load inwards, lose overall lift and potentially increase drag, but are able to counter this with reduced bending stress. As outer wing twist is increased, the lift to drag ratio is improved, but also to the detriment of bending moment. The experimental results illustrate that each configuration can justifiably offer strong specific range performance, indicating that perhaps a polar of optimal points throughout the flight envelope can be sought and achieved. Experimental results, representing take off conditions, also indicate that potentially the planar wing offers the peak specific air range result, whereas computational results, modelled to resemble flight cruise conditions, favour high dihedral, low twist configurations. These results further reinforce the belief that there are unique and contrasting optimal range schedules for each phase of the flight envelope.

In order to advance these findings, computational results will be generated to replicate wind tunnel conditions to give a closer basis for comparison. In addition, further wind tunnel testing is to be undertaken over a wider range of configura-

tions to ascertain the effects of cross coupling the two morphing features. Pressure readings will also be utilised at discrete spanwise locations in order to examine the change in local load across the wing. Finally, a more detailed weight estimation, based upon the measured forces and moments, is required to aid the comparison with optimisation results based upon a wing sizing algorithm. As has been witnessed, the formulation of this aspect of the results can have a significant impact on determining the overall effectiveness of each geometry.

6 Acknowledgements

This paper presents follow-on work from the MORPHLET Research Group in collaboration with EPSRC and Airbus UK.

References

- [1] R. T. Whitcomb, "A design approach and selected wind-tunnel results at high subsonic mounted speeds for winglets," *NASA TN D-8260*, July 1976.
- [2] M. J. Smith, N. Komerath, R. Ames, and O. Wong, "Performance analysis of a wing with multiple winglets," *AIAA Applied Aerodynamics Conference, 2001-2407*, 2001.
- [3] U. La Roche and S. Palffy, "Wing-grid, a novel device for reduction of induced drag on wings," *International Congress of The Aeronautical Sciences (ICAS)*, 1996.
- [4] S. A. Ning and I. Kroo, "Tip extensions, winglets, and c-wings: conceptual design and optimization," *Stanford University, Stanford, CA*.
- [5] D. D. Smith, A. T. Isikveren, R. M. Ajaj, and M. I. Friswell, "Multidisciplinary design optimization of an active non-planar polymorphing wing," *27th International Congress of The Aeronautical Sciences (ICAS)*, September 2010.
- [6] D. D. Smith, A. T. Isikveren, R. M. Ajaj, and M. I. Friswell, "Multiobjective optimization for the multi-phase design of active polymorphing wings," *AIAA Journal*, vol. 49, no.4, July - August 2012.
- [7] L. Prandtl, "Applications of modern hydro-

dynamics to aeronautics,” *NACA Report 116*, 1921.

- [8] S. C. Smith, “A computational and experimental study of nonlinear aspects of induced drag,” *NASA TR 3598*, 1996.
- [9] D. Schwamborn, A. D. Gardner, H. von Geyr, A. Krumbein, and H. Lüdecke, “Development of the DLR tau-code for aerospace applications,” *Proceedings of the International Conference on Aerospace Science and Technology, Bangalore, India, 26-28 June 2008*.
- [10] <http://larosterna.com/sumo.html> July 2012.
- [11] J. B. Barlow, W. H. Rae Jr, and A. Pope, *Low Speed Wind Tunnel Testing, 3rd Edition*. Wiley-Interscience, 1999.
- [12] http://www.ambercomposites.com/downloads/datasheet/wb-1222_tds_gb.pdf July 2012.
- [13] <http://www.cetl.org/Images/Fortus360mc/ABS-M30SpecSheet.pdf> July 2012.

6.1 Copyright Statement

The authors confirm that they, and/or their company or organization, hold copyright on all of the original material included in this paper. The authors also confirm that they have obtained permission, from the copyright holder of any third party material included in this paper, to publish it as part of their paper. The authors confirm that they give permission, or have obtained permission from the copyright holder of this paper, for the publication and distribution of this paper as part of the ICAS2012 proceedings or as individual off-prints from the proceedings.